Organ-specific mercury stable isotopes, speciation and particle measurements reveal methylmercury detoxification processes in Atlantic Bluefin Tuna

Martin Wiech, André M Bienfait, Marta Silva, Julien Barre, Veronika Sele, Michael S Bank, Sylvain Bérail, Emmanuel Tessier, David Amouroux, Atabak M Azad

Journal of Hazardous Materials 473 (2024) 134699

Contents lists available at ScienceDirect

Journal of Hazardous Materials

journal homepage: www.elsevier.com/locate/jhazmat

Organ-specific mercury stable isotopes, speciation and particle measurements reveal methylmercury detoxification processes in Atlantic Bluefin Tuna

Martin Wiech [a,*], André M. Bienfait [a], Marta Silva [a], Julien Barre [b], Veronika Sele [a], Michael S. Bank [a,c], Sylvain Bérail [b], Emmanuel Tessier [d], David Amouroux [d], Atabak M. Azad [a]

[a] Institute of Marine Research, Bergen, Norway
[b] Advanced Isotopic Analysis, Pau, France
[c] University of Massachusetts Amherst, Amherst, MA, USA
[d] Université de Pau et des Pays de l'Adour, E2S UPPA, CNRS, IPREM, Institut des Sciences Analytiques et de Physico-chimie pour l'Environnement et la Matériaux, Pau, France

HIGHLIGHTS

- Hg stable isotopes and Hg/Se species were measured in 13 tissue types of ABFT.
- We found evidence for organ-specific *in vivo* Hg-demethylation and biomineralization.
- The lowest δ^{202}Hg values and %MeHg were found in the spleen and kidney.
- Particulate Hg and Se were detected in all tissues analyzed: spleen≈kidney> >muscle.
- Se particles not associated with Hg were present in spleen and kidney.

GRAPHICAL ABSTRACT

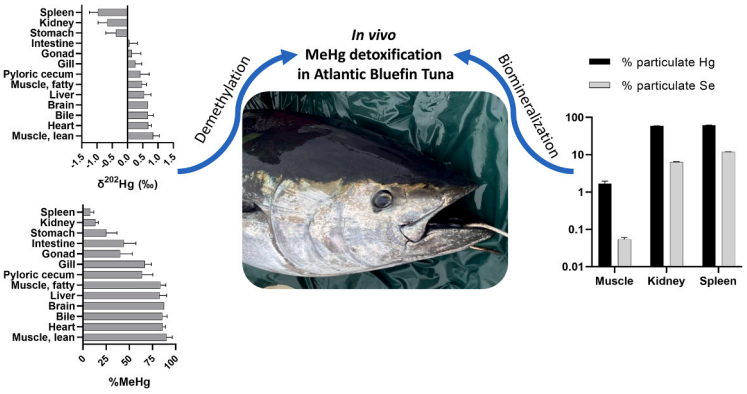

ARTICLE INFO

Keywords:
Mercury
Fish
Tiemannite
Demethylation
Biomineralization

ABSTRACT

Identifying metabolism and detoxification mechanisms of Hg in biota has important implications for biomonitoring, ecotoxicology, and food safety. Compared to marine mammals and waterbirds, detoxification of MeHg in fish is understudied. Here, we investigated Hg detoxification in Atlantic bluefin tuna *Thunnus thynnus* using organ-specific Hg and Se speciation data, stable Hg isotope signatures, and Hg and Se particle measurements in multiple tissues. Our results provide evidence for *in vivo* demethylation and biomineralization of HgSe particles, particularly in spleen and kidney. We observed a maximum range of 1.83‰ for δ^{202}Hg between spleen and lean muscle, whereas Δ^{199}Hg values were similar across all tissues. Mean percent methylmercury ranged from 8% in spleen to 90% in lean muscle. The particulate masses of Hg and Se were higher in spleen and kidney (Hg: 61% and 59%, Se: 12% and 6%, respectively) compared to muscle (Hg: 2%, Se: 0.05%). Our data supports the hypothesis of an organ-specific, two-step detoxification of methylmercury in wild marine fish, consisting of

* Corresponding author.
E-mail address: Martin.Wiech@hi.no (M. Wiech).

https://doi.org/10.1016/j.jhazmat.2024.134699
Received 12 January 2024; Received in revised form 24 April 2024; Accepted 21 May 2024
Available online 22 May 2024

demethylation and biomineralization, like reported for waterbirds. While mass dependent fractionation signatures were highly organ specific, stable mass independent fractionation signatures across all tissues make them potential candidates for source apportionment studies of Hg using ABFT.

1. Introduction

Mercury (Hg) is a widespread, environmental pollutant with potential toxic effects and negative implications for ecosystems and public health [1-3]. Methylmercury (MeHg) is a potent neurotoxin and easily transferred within and among food webs and is often the dominant species in marine fish fillet [4–7]. In aquatic environments, inorganic Hg can be methylated in biotic and abiotic ecosystem compartments specifically within sediments and the water column [8-10]. MeHg enters aquatic food webs primarily through dietary pathways and biomagnifies and bioaccumulates over the lifespan of biota, including marine fish at high trophic positions [11-14].

Atlantic bluefin tuna (ABFT- *Thunnus thynnus*) are large apex predators inhabiting Atlantic waters and can grow to over 3 m in length with a maximum life span of approximately 50 years [15,16]. Due to the large size and age of ABFT and long half-life of MeHg in fish, high concentrations of MeHg in this species are relatively common [17-19]. High MeHg concentrations are a considerable food safety concern, especially since ABFT is an appreciated global commodity and is widely consumed by humans. Health based guidance values and maximum levels for Hg in food, as well as consumption advisories for this species are established to assure food safety (*e.g.* Rice et al., [20,21]). The high MeHg concentrations in bluefin tuna and their long-lived nature make them an ocean biomonitoring species that can be used for identifying large-scale spatiotemporal Hg trends [18,19]. MeHg also induces toxic effects in fish on multiple levels including neurotramsission, oxidative stress, behaviour and morpho-structural changes in the central nervous system [22], and detoxification mechanisms are important in the context of further understanding toxicokinetic processing of this ubiquitous pollutant.

Methylmercury is primarily stored in muscle, bound to thiol groups comprised of protein incorporated cysteine residues in methylmercury-L-cysteinate (MeHgCys) complexes and thereby may offer protection to other organs [23,24]. Demethylation of MeHg has been suggested as another important detoxification mechanism and evidence exists that it occurs across a wide array of aquatic organisms including mammals [25-27] and waterbirds [28-30], while it is less studied in fish.

Mercury stable isotope ratios are promising tools to reveal key metabolic processes in biota especially regarding demethylation, as mass dependent fractionation (MDF) occurs due to the retention of isotopically heavier Hg during *in vivo* demethylation of MeHg [31,32]. Reviewing and integrating existing literature on Hg stable isotopes in biota, Li et al. [33], established a conceptual model of Hg distribution and transformation in birds supported by synchrotron-based X-ray analyses [29,34]. Detoxification was outlined as a two-step reaction from MeHg to Hg-selenide (HgSe). First, a demethylation of MeHg to mainly a $Hg(selenocysteine)_4$ complex ($Hg(Sec)_4$), associated with selenoprotein P (SelP) and accompanied by MDF and a negative change of $\delta^{202}Hg$ values. Second, biomineralization to chemically inert nanoparticulate mercury selenide (HgSe) with a potitive shift in $\delta^{202}Hg$ [29,35]. Also in whales, there is convincing evidence for *in vivo* demethylation of MeHg, as reviewed by Li et al., [33] as well as the presence of biomineralized particulate HgSe [26,36]. In fish, detoxification processes of MeHg and the involvement of different tissues is understudied and existing literature inconclusive [37-41]. However, more recent studies found evidence for demethylation [42,29,43-47]. Considering the biomineralization of HgSe particles as a consecutive part of MeHg demethylation [33], the presence of HgSe particles can be considered a reliable proxy for *in vivo* demethylation. To our knowledge, only two studies measured Hg-nanoparticles in fish and detected particles in muscle [35,48]. The formation of Hg and Se containing particles and compounds might influence the levels of different Se species. In pilot whales it was shown, that selenomethionine (SeMet) was depleted in liver of adults compared to juveniles, as a consequence of MeHg detoxification [26].

In this study, multiple analytical tools were applied to investigate the MeHg metabolism and shed light on the detoxification mechanisms in ABFT. The Hg speciation and stable isotope analyses were performed on 13 different tissues, in addition to Se speciation and Hg and Se particle measurements in three different tissues. Specifically, we tested the *a priori* prediction that organ-specific demethylation is taking place and will result in HgSe particle formation in ABFT.

2. Material and methods

2.1. Fish and organ sample collection

Nine adult Atlantic bluefin tuna *Thunnus thynnus* measuring 250 ± 15 cm (Mean ± SD straight fork length) and an estimated age of 15.8 ± 2.4 years (according to Cort, Estruch [49]), were caught by recreational fishers with rod and line from August-October 2019/2020 along the Norwegian coast (Table S1) with permission from the Norwegian Directorate of Fisheries. During Autumn, ABFT inhabit the Norwegian coast for foraging, after spawning mainly in the Mediterranean Sea during summer. Samples were taken fresh on-site when the fish were landed. Lean and fatty muscle, gill (filaments only), and kidney samples were taken with clean sampling devices and stored frozen in clean, sterile, plastic bags until analysis. Further, whole viscera were frozen and sent to the laboratory at the Institute of Marine Research, Bergen, Norway for dissection under clean conditions using powder free nitrile gloves, and clean, stainless steel sampling devices. Liver, spleen, gonad, and heart were sampled and blotted dry. From intestine, pyloric cecum and stomach, tissue samples were taken avoiding the content, focusing on the actual tissue. For bile, only the liquid part was taken. All samples were homogenized before and after freeze-drying except bile, which was measured wet and freeze dried afterwards to be able to display all values based on a dry weight basis. For particle analyses, homogenized wet tissue samples were used.

2.2. Chemical analysis

2.2.1. Total mercury and selenium

Mercury and selenium concentrations were analyzed by Inductively Coupled Plasma Mass Spectrometry (7800 ICP MS, Agilent technologies). The samples were freeze dried and mixed to a homogeneous powder. An aliquot of the sample was digested in a nitric acid and hydrogen peroxide mixture on a regulated heating block (Digiprep, SCP Science) for 6 h. Prior to total concentration analysis, samples were diluted in ultrapure water. The calibration for Hg and Se were performed using the standard addition methodology [50] prepared in a pool of samples to prevent matrix effects. Se concentrations were determined using the reaction cell mode with hydrogen to avoid any polyatomic interferences (Ar, Ca, Cl *etc.*). To prevent and control for a memory effect of mercury, specific conditioning with hydrochloric and nitric acid solution with a background monitoring was performed. To assess the accuracy of the method, three certified reference materials (CRM) including DOLT-5, TORT-3 and CE-464 were analyzed and the measured concentrations (n = 3) agreed with the certified values for both Hg and Se with a maximum average deviation of 7% to the certified concentrations (Table S2).

2.2.2. Mercury speciation

The methylmercury and inorganic mercury (IHg) contents were determined by double spike species-specific isotope dilution analysis (SSID) and gas chromatography-inductively coupled plasma-mass spectrometry (GC-ICP-MS) analysis [51,52]. Depending on the sample type, soft extraction with 6 N HNO_3 or tetramethylammonium hydroxide was achieved on a microwave assisted extraction at 75 °C (Discover-S, CEM). The extracts were spiked with appropriate amount of isotopically enriched ^{199}IHg and ^{201}MeHg (ISC-Science). A derivatization reaction with $NaBPr_4$ at controlled pH (3.9) followed by a liquid/liquid extraction in iso-octane was then conducted. Finally, the samples were analyzed by GC-ICP-MS (Trace GC Ultra coupled to XSeries II ICP-MS, Thermo Scientific, Waltham, USA) and the results were calculated as previously detailed elsewhere [37,53]. Three reference materials with certified MeHg composition including DOLT-5, TORT-3 and CE-464 have been analyzed in triplicate to assess the accuracy of the methods and measured concentrations for the three CRMs were in line with the certified values with a maximum average measured deviation of 12% to the certified concentrations (Table S3).

2.2.3. Particle analysis

To measure particulate mercury (pHg) and selenium (pSe), a subset of tissues was selected for single particle inductively coupled plasma mass spectrometry (sp-ICP-MS). Muscle, kidney, and spleen were chosen with the lowest and highest %MeHg and each sample was analyzed in triplicate. The homogenized tissues were enzymatically digested using Protamex® (Supplementary section 4.2 "Enzymatic digestion") based on an in-house developed protocol [54], before introduction into the ICP-MS. After initial screening (Supplementary section 4.1 "Initial screening"), dilution factors of 5 000, 10 000 and 20 000 were used for muscle, kidney, and spleen tissue, respectively. High dilution factors were chosen to a) reduce the baseline signal caused by dissolved (ionic) Hg, and b) reduce the probability of particle signals overlapping in the time-resolved spectra. A data collection time of two minutes delivered a satisfactory number of Hg- based particle events for all tissues. Representative time-resolved spectra of ^{78}Se and ^{202}Hg from the sp-ICP-MS analyses are shown Fig. S1 and S2. The LOQ_{number} represents the minimum number of particle events that needs to be detected within an experiment to quantify the amount of particles in the studied sample. The LOQ_{number} was estimated from particle events detected in blanks, using the 10σ-approach, resulting in 15 events within 120 s for Se-based measurements and 19 for Hg-based ones. Detailed information on quality assurance/quality control (QA/QC), including spiking with gold nanoparticles and use of ionic standards, is presented in supplementary section 4.3 "QA/QC".

All sp-ICP-MS measurements were performed on an Agilent 8900 triple quadrupole inductively coupled plasma mass spectrometer (Agilent Technologies Inc., Santa Barbara CA/USA) with reaction and collision gas capability (see Table S4 for details). Samples were analyzed in the time resolved single particle mode, set up in the nanoparticle extension of the Masshunter software (Agilent Technologies Inc., CA/USA; Version 5.1).

2.2.4. Selenium speciation

Selenium speciation analysis was performed in duplicates on muscle, spleen, and kidney of three different ABFT individuals. The extraction procedure for organic Se species was based on the method described by Sele et al. [55] and Vaksdal [56]. In short, the sample was digested with cellulase and protease in a water bath (37 °C, 20 h, at 100 rpm). The extracts obtained were separated by centrifuging at 3500 rpm for 10 min. Soluble and non-soluble fractions were kept separately. The soluble fraction was filtered and analysed by high performance liquid chromatography (HPLC, 1260 HPLC) coupled to ICP-MS (7900 ICP-MS, both Agilent Technologies, CA, USA). The organic Se species were separated using the chromatographic and ICP-MS settings described in Table S5. Selenomethionine (SeMet) was quantified using an external calibration curve of SeMet, using Seleno-DL-methionine (Sigma-Aldrich, Norway) prepared in Milli-Q water. Accuracy of results was verified analyzing two CRMs (ERM BC210a and SELM-1) in duplicate and the maximum average deviation of the measured values to the verified values was 3%. Data obtained are presented in Table S6.

The total Se concentrations in the soluble and non-soluble fractions were determined by ICP-MS using a procedure described previously [57]. Briefly, the soluble fraction (1 mL) was digested with HNO_3 (5% w/w) in an UltraWAVE (Milestone, Italy) and diluted to 25 mL with Milli-Q water. The non-soluble fractions were dried (70 °C, 24 h) in an oven, then the dried material was weighed, acid-digested in an UltraWAVE, and diluted to 25 mL with water. The samples were analysed by ICP-MS (iCapQ ICP-MS, Thermo Scientific, Waltham, USA) equipped with an auto sampler (FAST SC-4Q DX, Elemental Scientific, Omaha, USA). The instrumental settings are described in Table S7. The quantification was performed with an external calibration curve of Se in a multielement standard (Teknolab, Oslo). Two CRMs (OT and TORT-3) were analyzed in duplicateto assess the accuracy of the method and the measured concentrations agreed with the certified values with a maximum average deviation of 4% (Table S8).

2.2.5. Mercury stable isotopes

Prior to Hg stable isotope analyses, samples were digested in a mixture of HNO_3/HCl/H_2O_2 (3:1:1) and heated at 90 °C on a hotplate for 48 h. Mercury isotopes analyses were performed using a cold vapor generation (CVG) with $SnCl_2$ reduction, coupled to a multicollector-ICP-MS (Nu Plasma, Nu Instruments). To correct the instrumental mass-bias, sample standard bracketing with NIST 3133 standard solution was used [58]. All the samples and standards were diluted to match a Hg concentration of 1 ng g^{-1}. Mass-dependent fractionations (MDF) of mercury were reported as recommended by Bergquist and Blum [59] relative to the NIST 3133 Hg solution as follows:

$$\delta^{xxx}Hg = \left(\frac{^{xxx/198}Hg_{sample}}{^{xxx/198}Hg_{NIST3133}} - 1 \right) * 1000‰$$

where xxx is the studied isotopes. Mass-independent fractionation (MIF) of Hg is reported as the difference between the theoretical value predicted by MDF and the measured values as Δ^{XXX}Hg in ‰ according to Bergquist and Blum [59]:

$$\Delta^{xxx}Hg = \delta^{xxx}Hg - \left(\delta^{202}Hg \times \beta_{xxx}\right)$$

where β_{xxx} is the kinetic mass-dependent scale factor, characteristic of the isotope which values are 0.2520 for ^{199}Hg, 0.5024 for ^{200}Hg, 0.7520 for ^{201}Hg and 1.493 for ^{204}Hg [59].

Analytical uncertainty for CVG/MC-ICP-MS was evaluated by multiple measurements of secondary standards and certified reference materials including measurements of NIST 9610 (n = 30), ERM CE 464 (n = 6), TORT-2 (n = 6) and NIST 1947, and our measurements were in agreement with certified values and previous findings [60,61] (Table S9).

2.2.6. Data curation

To statistically evaluate differences of the different forms of Hg, and stable isotope signatures (δ^{202}Hg and Δ^{199}Hg) between the different organs, one-way ANOVA was performed followed by Tukey's honest significant difference test. The significance threshold was set to $p < 0.05$. Normal distribution was checked using Shapiro-Wilk test and Q-Q plot. The Kolmogorov-Smirnov test was used to assess the normality of residuals. Spearman correlation was used to investigate the relationship between length and %MeHg in different organs and %MeHg and δ^{202}Hg. To evaluate relationships between the different isotopic signatures standard linear regression was used. The data were treated, and figures created in R (version 4.2.1) operated in RStudio (version 2022.07.2+576; RStudio Team, 2022) and using GraphPad Prism

version 8.3.0 for Windows, GraphPad Software, San Diego, California. If not mentioned otherwise, means ± standard deviations are given in the text.

3. Results and discussion

3.1. Total mercury in muscle

The mean THg in lean muscle tissue of ABFT from this investigation was 0.70 ± 0.26 mg/kg w.w. (Mean ± SD), and concentrations in fatty muscle tissue were slightly lower (0.59 ± 0.34 mg/kg w.w.). Since tuna are widely consumed as seafood, they are subject to trade and export controls for several contaminants including Hg, and the measured concentrations are below the current maximum level (mL) in the European Union (EU) designated by the Commission Regulation (EU) 2023/915 and set to 1.0 mg THg/kg w.w. European Commission [62]. Considering the size of the measured ABFT (250 ± 15 cm), our data are similar to ABFT concentrations in individuals from Northwest Atlantic, reported by Lee et al. [18] with an average of 0.76 ± 0.33 mg/kg w.w. for fish with an average curved fork length (CFL) of 218 ± 30 cm. However, a study on wild ABFT caught in the Mediterranean Sea reported much higher values of 1.7 ± 0.2 mg/kg w.w. in much smaller individuals (135 ± 23 cm CFL) [17]. In a global study on bluefin tuna, Tseng et al. [19] reported ocean basin specific THg concentrations and that highly exposed individuals from the Mediterranean Sea reflected regional contamination and/or the production and food web bioavailability of MeHg. Furthermore, these investigators also reported that only a minor fraction of ABFT from this region is migrating to the North Atlantic Ocean [19]. However, it has been shown that most of the fish caught along the Norwegian coast originate from the Mediterranean Sea [63]. The Hg concentrations of ABFT sampled in the Northwest and Northeast Atlantic spawning at different sites [63] are similar, while the concentrations in tuna caught in the Mediterranean Sea are much higher. This indicates that fish from the Northwest Atlantic Ocean, originating mostly from the population spawning in the Gulf of Mexico, and fish caught in the Northeast Atlantic are likely experiencing more similar Hg exposure regimes compared to non-migrating fish and migrating fish from the same Mediterranean population.

3.2. Organ-specific distribution of mercury species

Here we provide Hg speciation data for 13 different ABFT tissues. Lean muscle had moderate THg concentrations (2.5 ± 1.5 mg/kg d.w.), whereas spleen samples had the highest THg concentrations with 32.3 ± 15.8 mg/kg d.w. followed by kidney with 21.2 ± 9.6 mg/kg d.w. being three times higher than the next highest organ, stomach with 6.8 ± 2.9 mg/kg d.w. (Table 1). Gills had the lowest THg concentrations (0.5 ± 0.1 mg/ kg d.w.). The remaining organs had mean THg concentrations between 1.4 and 4.0 mg/kg d.w. This suggests that kidney, spleen and potentially stomach are important organs for the Hg accumulation, metabolism and potential detoxification in ABFT. Concentrations in liver tissue were highly variable (3.5 ± 3.0 mg/kg d.w.). Muscle tissue also plays an important role in Hg metabolism and is the primary MeHg storing tissue in ABFT considering its size relative to other tissues. MeHg comprised 90 % of THg in lean muscle tissues (Table 1), where it is present as less toxic MeHgCys [24]. The lowest % MeHg were found in stomach, kidney, and spleen with a mean of 25 ± 12 %, 14 ± 3 % and as low as 8 ± 4 %, respectively. Furthermore, we observed high concentrations of inorganic mercury (IHg) between 5.1 ± 2.8 mg/kg d.w. in stomach and 29.9 ± 15.4 mg/kg d.w in spleen. Liver samples contained primarily MeHg (66 - 91 %), which contrasts with earlier findings for tusk *Brosme brosme,* with a %MeHg in liver as low as 14 – 52 % [45]. For small marine pelagic sardine species, % MeHg in liver was low with 20–50 %. In freshwater fish Northern Pike *Esox lucius*, a %MeHg of 28–51 % was reported in livers with THg > 0.5 mg/kg w.w. [64] and in liver of spotted gar *Lepisosteus oculatus* the MeHg contribution was on average as low as 2 % [65], while it was 74 % and 56 % in Largemouth bass *Micropterus salmoides* and Red-ear sunfish *Lepomis microlophus,* respectively. This may indicate that different fish species use different tissues for Hg detoxification and IHg storage. The use of different Hg speciation methods across investigations may also add uncertainty when comparing %MeHg data.

Some authors hypothesized that high ratios of IHg in liver might be due to dietary accumulation of IHg [64], while others interpreted them as a sign of the occurrence of *in vivo* demethylation happening [65]. However, as Wang et al. [47] were able to show *in vivo* demethylation in a marine fish in a lab study, the presence of such high concentrations of the less bioavailable IHg may, at least partly, be attributed to *in vivo* demethylation. They reported the demethylation taking place in the liver being slow and not of significance for the whole fish Hg level in black seabream *Acanthopagrus schlegeli*, while the activity in the intestine was substantially higher. This is in accordance with results of our study with a higher ratio of MeHg in liver than in the intestine. However, our results show even lower MeHg ratios in other organs, especially kidney, spleen, and stomach, suggesting a high rate of demethylation in these tissues, or potentially, that the IHg originating from demethylation in other organs including liver, is accumulating in these organs. This is also supported by a finding in Arctic char *Salvelinus alpinus* fed with inorganic ^{203}Hg. There, 50 % of ingested IHg was eliminated quickly (4–7 days) and most of the retained Hg was retained in the gut. Only a small amount was distributed further [66], potentially meaning that especially high concentrations of IHg in spleen and kidney is likely not due to accumulation from food, and can be considered a product of *in vivo* demethylation. The %MeHg in liver is highly variable and these

Table 1
Concentrations of total Mercury (THg), inorganic mercury (IHg), methyl mercury (MeHg), total selenium (Se), the selenium to mercury molar ratio (Se:Hg) and mass-dependent and Hg isotope composition (δ^{202}Hg and Δ^{199}Hg) in different tissues of Atlantic bluefin tuna caught off the coast of Norway. Mean ± standard deviation is presented.

Tissue	n	THg	IHg	MeHg	TSe	%MeHg	Se:Hg	δ^{202}Hg	Δ^{199}Hg
		mg·kg^{-1} dry weight				%	molar ratio	‰	
Spleen	9	32.3 ± 15.8	29.9 ± 15.4	2.3 ± 1.0	343 ± 107	8 ± 4	30 ± 11	-0.97 ± 0.28	1.43 ± 0.11
Kidney	4	21.2 ± 9.6	18.5 ± 9.1	2.8 ± 0.9	64.0 ± 13.4	14 ± 3	8 ± 3	-0.66 ± 0.3	1.30 ± 0.06
Stomach	9	6.8 ± 2.9	5.1 ± 2.8	1.6 ± 0.8	20.5 ± 5.5	25 ± 12	10 ± 7	-0.38 ± 0.33	1.37 ± 0.14
Intestine	9	4.0 ± 2.0	2.3 ± 1.2	1.7 ± 0.9	13.1 ± 2.8	44 ± 13	10 ± 6	0.06 ± 0.27	1.42 ± 0.1
Gonad	9	1.5 ± 2.2	0.8 ± 1.2	0.6 ± 1.1	4.3 ± 5.4	40 ± 13	21 ± 15	0.14 ± 0.3	1.39 ± 0.08
Gill	6	0.51 ± 0.11	0.23 ± 0.07	0.5 ± 0.1	7.1 ± 3.0	67 ± 7	39 ± 21	0.26 ± 0.21	1.38 ± 0.08
Pyloric cecum	7	3.3 ± 3.3	1.1 ± 1.1	2.3 ± 2.3	8.9 ± 5.4	64 ± 12	10 ± 5	0.42 ± 0.29	1.36 ± 0.1
Muscle, fatty	8	1.4 ± 1.0	0.3 ± 0.2	1.1 ± 0.8	2.4 ± 1.2	84 ± 6	6 ± 2	0.47 ± 0.16	1.35 ± 0.07
Liver	9	3.5 ± 3.0	0.8 ± 1.0	2.7 ± 2.0	40.1 ± 15.9	83 ± 8	44 ± 23	0.54 ± 0.23	1.42 ± 0.13
Brain	1	0.8	0.1	0.7	16.9	87	52	0.67	1.51
Bile	7	1.5 ± 0.7	0.2 ± 0.1	1.2 ± 0.6	28.6 ± 15.7	86 ± 5	67 ± 54	0.67 ± 0.18	1.40 ± 0.15
Heart	7	2.8 ± 0.9	0.4 ± 0.20	2.4 ± 0.7	19.0 ± 4.3	86 ± 3	19 ± 8	0.68 ± 0.11	1.46 ± 0.12
Muscle, lean	9	2.5 ± 1.5	0.3 ± 0.3	2.1 ± 1.2	3.6 ± 2.9	90 ± 6	5 ± 4	0.84 ± 0.2	1.44 ± 0.2

differences may be partly driven by the degree of contamination [44,45]. For tusk, a high degree of Hg pollution was correlated with low %MeHg in liver ranging from 14 to 52 % [45]. Also for European seabass, %MeHg in liver varied substantially from 7 to 70 % in different populations throughout Europe correlating with the degree of contamination, while %MeHg values in muscle were constant [44]. The relatively high %MeHg found in the ABFT liver might therefore indicate that our fish were mainly foraging in less contaminated areas. This is rather likely, considering their large-scale foraging range and since they were caught offshore the Norwegian coast. However, the pelagic lifestyle of ABFT also may play a role since the IHg contamination often takes place in benthic food webs associated with seafloor sediments [13,67]. As a result of demethylation of MeHg over time, %MeHg in liver can also decrease with age, as shown for pilot whales [25]. No significant correlation was found between %MeHg and length in any of the ABFT organs ($p \geq 0.24$ for all organs). However, this might be caused by the low n, relatively low length variation in our dataset, and as length is only a proxy for empirical age.

3.3. Organ distribution of particulate Hg and Se

We were able to detect particulate mercury (pHg) and selenium (pSe), presumably HgSe, in all analyzed tissues, including spleen, kidney, and lean muscle, containing different concentrations and sizes of HgSe particles (Fig. 1). To our knowledge, there are only two other investigations reporting the presence of nano-sized Hg-containing particles in fish [35,48]. In both studies, only muscle tissue was analyzed and Suzuki et al. [48] detected no signals of pSe. Our study shows the presence of naturally occurring Hg and Se particles in three organs of ABFT: muscle, kidney, and spleen. The findings revealed a large difference in the mass ratio of particulate Hg and Se to total Hg (%pHg) and Se (%pSe), detected by sp-ICP-MS, in spleen and kidney compared to muscle tissue. For Hg the difference was largest with as much as 61 % and 59 % of the detected mass of Hg in spleen and kidney being present as particles, while only 2 % of the detected Hg in muscle was present as particles (Fig. 1). For Se, a similar trend was found with 12 % and 6 % particles in spleen and kidney, respectively, compared to muscle with 0.05 %. This indicates that the higher concentrations of IHg in kidney and spleen were mainly present in particulate form, presumably as HgSe (nano-)particles and as proposed earlier also as $Hg(Sec)_4$ [29]. The large difference between %pHg and %pSe can be ascribed to Se being bound to proteins. It can therefore be assumed that only minor amounts of total Se in spleen and kidney of ABFT are involved in the biomineralization of Hg. In blue Marlin muscle, Manceau et al. [35] found equally high proportions of HgSe particles as we did in kidney and spleen of ABFT, and also the %MeHg was equally low. Also, the number of particles per mass followed the same trend for both Hg and Se with the highest numbers of Hg-containing particles in spleen with $250.0{\cdot}10^7 \pm 7.3{\cdot}10^7$ Hg particles·g^{-1} w.w. and kidney with $167.4{\cdot}10^7 \pm 2.4{\cdot}10^7$ Hg particles·g^{-1} w.w., and much lower numbers in muscle with $9.6{\cdot}10^7 \pm 1.0{\cdot}10^7$ Hg particles·g^{-1} w.w. (Fig. 1). The number of detected Se-containing particles was lower but still showed the same trend among organs with higher numbers in spleen and kidney with $235.7{\cdot}10^7 \pm 13.8{\cdot}10^7$ and $36.9{\cdot}10^7 \pm 0.5{\cdot}10^7$ Se particles·g^{-1} w.w., compared to only minor amounts in muscle ($1.42{\cdot}10^5 \pm 4.53{\cdot}10^3$ Se particles·g^{-1} w.w.), which should be considered $<LOQ_{number}$. We consider the similarity of the occurrence patterns of Hg- and Se-containing particles a good indicator of the presence of HgSe particles in different organs of ABFT. Likely, they are formed following *in vivo* MeHg demethylation similarly as suggested for mammals [26] and seabirds [34,68], exhibiting *in vivo* MeHg demethylation. Even muscle tissue with high %MeHg, contained particles as also reported for marine mammals [69,70]. In muscle tissue of European Seabass *Dicentrarchus labrax* exposed to moderate levels of MeHg, changes in δ^{202}Hg indicated Hg detoxification activity [43], possibly resulting in biomineralization. However, redistribution of biomineralized HgSe from other organs and internalization of HgSe particles *via* the diet cannot be ruled out, even though dietary uptake was not detected in rats [71].

The number of Hg-containing particles per mass reported by Suzuki et al. [48] for muscle of individuals of their tuna-swordfish group was comparable to our findings, considering differences in sample preparation and instrument settings (17.7 *vs.* $9.6 \pm 1.0{\cdot}10^7$ particles·g^{-1} w.w.). In spleen and kidney, our counts of Hg-containing particles were significantly higher. Our measured mean particle size (assuming solid spherical HgSe particles with a density of 8.27 g/cm^3, particle detection threshold ~24.5 nm [PDT/LOQ_{size}], background equivalent diameter [BED] ~10 nm, monitored isotope ^{202}Hg) in muscle tissue of 27.9 ± 0.1 nm is virtually identical to the earlier reported 29 nm in tuna muscle [48]. In spleen and kidney, the mean particle size was somewhat larger with 44.0 ± 0.2 and 42.5 ± 0.0 nm, respectively (See Fig. S3 for particle size distributions). It is important to note that sp-ICP-MS is generally not able to measure the entire particle size distribution due to methodological restrictions, such as instrumental sensitivity and/or elevated background from dissolved species, as also reported earlier by others [48]. Since the sensitivity of the instrumentation for Se was significantly lower compared to Hg, the LOQ_{size} increased to about 86 nm, with a BED of ~34 nm. Based on the Se-measurements, the mean HgSe particle sizes were larger with on average 107.5 ± 0.7 and 111.6

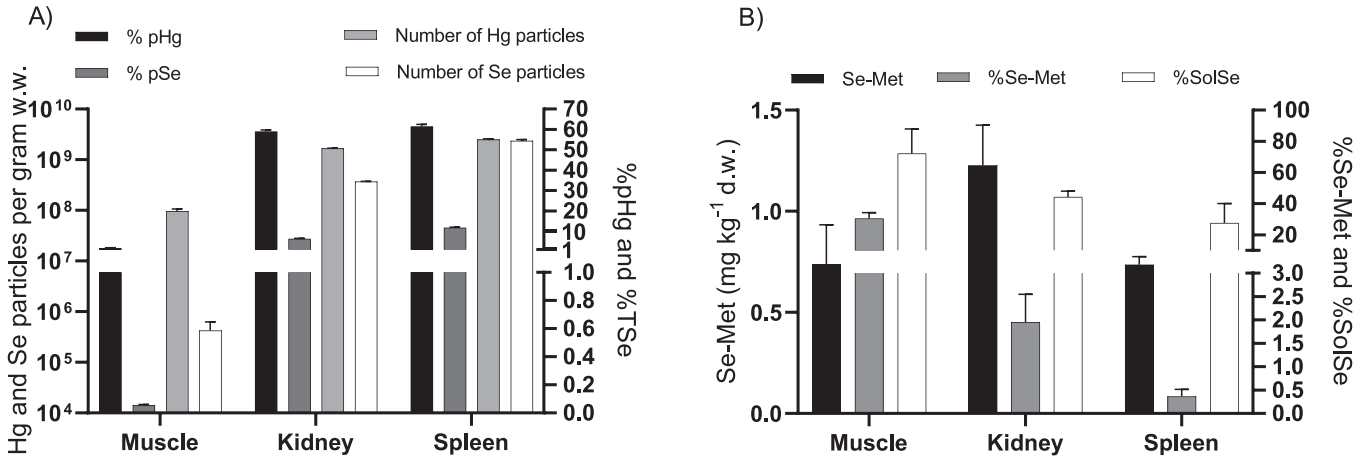

Fig. 1. Particle distribution and Se-Met in lean muscle, kidney and spleen of Atlantic bluefin tuna caught at the Norwegian coast. Panel A) shows the ratio of measured particulate to the detected total amount of Hg (% pHg) and Se (% pSe) and the number of detected particles in the different organ tissues in particles/g w.w.. Panel B) shows the measured concentration (based on dry weight) of Se-methionine (Se-Met) and the ratio of Se-Met to total Se (%Se-Met) and fraction of TSe as protease-solubilized Se (%SolSe). Means ± standard deviations are given.

± 1.0 nm in spleen and kidney, respectively. There were only 3.0 ± 1.4 particles detected in muscle during the Se measurement with a mean size of 134.2 ± 36.0 nm. The latter finding was to be considered below LOQ_{number}. For Hg- and Se-based measurements, the number of particles detected was increasing with decreasing particle size, peaking at or around the particle detection threshold, which represents a LOQ_{size}. This means that the real mean particle size will be somewhat lower for pHg and significantly lower for pSe. The single largest presumed HgSe particles detected in individual analyses based on monitoring Hg were 181 ± 11 nm, 180 ± 25 nm and 96 ± 26 nm for spleen, kidney, and muscle, respectively. Measurements in muscle are, as mean size, in good agreement with the 90 nm maximum size reported by Suzuki et al. [48]. However, based on Se measurements, the single largest presumed HgSe particles detected were in all cases significantly larger with 361 ± 22 nm, 260 ± 30 nm and 162 ± 17 nm, respectively. This mismatch indicates towards the largest Se-containing particles not being HgSe but a not-yet identified Se-based particle species. Also, the ratio of pSe to pHg points towards the existence of other Se-containing particles, after manually adjusting PDT for Hg to a comparable level as for Se. Considering the spleen samples measurements with optimized PDT for Hg and Se individually, we found the particle number ratio to be close to 1 (4305.7 (± 251.3) pSe: 4566.7 (± 134.1) pHg ≈ 0.94 pSe:pHg), as one would expect for HgSe particles. However, the PDT for Se is significantly higher, due to the lower sensitivity of the ICP-MS towards Se. This, on the other hand, results in a lower LOQ_{size} for pHg and causes more particles of the large fraction of small pHg present in the sample to fall into the measurable range. After raising the PDT for Hg to the same size limit as for Se, under the assumption of HgSe particles being measured, the number of pHg detected significantly decreased to 149.7 (± 21.5). This resulted in a pSe:pHg ratio of 28.8, which is close to the Se:Hg molar ratio of 26.4 measured in the respective individual. For kidney samples the trend is similar, however, less pronounced with the Se:Hg particle ratio changing from 0.22 to 5.83, ending up at roughly half of the Se:Hg molar ratio of 12.1 measured in the respective sample. This indicates the presence of a large amount of pSe, not associated with Hg. For muscle, too few particles were detectable to draw any conclusions. The high Se to Hg particle ratio in kidney and spleen suggests that selenium-containing particles of other trace elements than Hg are being formed, which could be addressed in future studies. An alternative explanation would be a non-stoichiometric particle composition of Hg_xSe_y, with $y >> x$. Compared to the findings in marine mammals [26, 70], our detected particles are much smaller in size. This might be due to higher concentrations of Hg in marine mammals and/or that the investigated animals were older, as larger and more particles were detected in adult pilot whales compared to the juveniles. The varying presence of HgSe particles in different organs has implications for our understanding of Hg concentrations, as it was shown that HgSe have low bioavailablity and toxicity [71], although some negative effects on immune system and lipid metabolism is reported in rodent models implying the importance for food risk assessment [72,73]. In blue Marlin muscle, a much higher proportion of IHg was found compared to ABFT and it was mainly complexed as $Hg(Sec)_4$ and HgSe, likely changing the bioavailability and toxicity of Hg significantly [35].

3.4. Organ distribution of selenium

The concentration of total selenium (TSe) varied substantially between the lean muscle, kidney, and spleen respectively equal to 2.4 ± 0.5, 66 ± 15, and 305 ± 125 mg/kg d.w. (Mean ± SD, n = 3). In contrast, the concentration of SeMet varied less with the highest concentrations in kidney (1.2 ± 0.3 mg/kg d.w.) and similar concentrations in lean muscle and spleen (0.75 ± 0.26 and 0.75 ± 0.09 mg/kg d.w. respectively) (Fig. 1). The concentrations of SeMet are in accordance with a previous speciation study, showing SeMet concentrations around 0.5 mg/kg in the edible part of longtail tuna *Thunnus tonggol* [74]. In pilot whales, it has been shown, that SeMet was depleted in liver and brain of adults compared to juvenile individuals, whereas Se-cysteine concentrations were maintained constant during time, and Se-cystathionine and inorganic Se concentrations were increased in adult individuals [26]. It has been argued that SeMet, which is considered the biological pool of Se, is used to mitigate the harmful effects caused by MeHg exposure, by providing a supply of Se which can bind to MeHg [75]. However, if the rate of binding of Se to MeHg is higher than the uptake, SeMet may become depleted [75]. It was hypothesized that MeHg toxicity is initially reflected in increased levels of SeCysteine intermediate species, followed by depletion of SeMet and lastly by a decrease in SeCysteine [26]. SeMet depletion might also have negative effects on fish health, as Se is an essential micronutrient required for metabolic processes in fish [76]. The SeCysteine was not analyzed in our study, due to methodological and instrument limitations. However, Se species other than SeMet were detected in the enzymatic extracts, particularly for the spleen and kidney tissues when analyzed by HPLC-ICP-MS, but not identified (Fig. S4).

Our results could not confirm a lower concentration of SeMet in tissues with high concentrations of HgSe particles (kidney and spleen) compared to a tissue with low particle concentrations (muscle) in adult ABFT. However, the ratio of SeMet to total Se is much higher in muscle tissue (30.9 ± 5.3 %) compared to kidney and spleen (2.0 ± 0.7 and 0.4 ± 0.2 %, respectively) (Fig. 1). Furthermore, total Se was determined in the enzymatic digests to assess how much Se was solubilized with protease (SolSe) for the different tissues, representing organic Se chemical forms [55]. The average recovery for SolSe fractions ranged from 27 to 72 %, with highest Se recovery for the muscle tissues (Fig. 1). The higher percentage of Se to total Se in the soluble protease extracts for the muscle tissue compared to kidney and spleen (Fig. 1) may be explained by these tissues having different structures and functions and containing other Se forms than muscle tissue. In muscle tissues of marine fish species, SeMet is often the major Se form [77]. Another organic Se form identified in muscle of tuna is selenoneine, accounting for up to 42 % of TSe [78]. Several Se chromatographic peaks, beside SeMet, were detected in the kidney and spleen of the ABFT (Fig. S4) suggesting the presence of low-molecular Se species, *e.g.* selenosugars, however, not identified. In a recent comprehensive study of the Se metabolism in rats, Se was found to accumulate as low-molecular weight selenosugars and as selenosugar-decorated proteins in the liver of the animals fed a graded diet of SeMet [79]. Overall, the lower ratio of SeMet to total Se for kidney and spleen combined with the higher HgSe particle concentrations in the same organs, may indicate that more Se is used for particle formation. This would then confirm previous hypotheses suggesting a potential role of SeMet in detoxifying MeHg [75]. The lower SolSe fractions for the kidney and spleen may also support the presence of more inorganic, or non-proteic forms of Se in these tissues, however, more studies are needed to confirm this.

The much higher Hg concentrations in marine mammals [26,69] compared to ABFT may induce a higher degree of detoxification and explain the higher extent of SeMet depletion and may also explain the much higher Se:Hg molar ratio observed in the tissues of ABFT. We observed Se:Hg molar ratios ranging from 4.6 ± 3.9 in lean muscle to 67.4 ± 54.1 in bile (Table 1). In whales, the Se:Hg molar ratio in adults was reported to be close to 1, and significantly higher in juveniles [26]. With accumulating Hg concentrations and parallel biomineralization of HgSe, the Se:Hg molar ratio of particle rich tissues will be dominated by the ratio in the particles, which is theoretically expected to be close to 1. This indicates, that the Hg concentrations and %pHg in ABFT tissues may not have been high enough to see a correlation between Se:Hg molar ratios and THg concentrations.

3.5. Organ-specific mercury isotope signatures

3.5.1. Mass-independent fractionation

The detected differences in $\delta^{202}Hg$ and stable $\Delta^{199}Hg$ signals

between organs suggest *in vivo* demethylation of MeHg in several organs of ABFT. Little variation was observed in Δ^{199}Hg between both, individual fish, and organs (Table 1) ranging between 1.3 and 1.5‰ ($F=0.81$, $p > 0.64$). It is widely accepted that no *in vivo* MIF is induced by the Hg metabolic processes in biota [33,80] and the low variation in Δ^{199}Hg observed within the wide set of tissues in ABFT suggests that the origin of Hg between organs and individual ABFT is similar, as reported earlier for internal organs of other marine taxa [25,81,30]. The low variability in MIF between the different organs in ABFT suggests that also less valuable and easier available tissues can be used for further studies on source apportionment using Hg stable isotope signatures. This is of importance when sampling ABFT tissues due to the high price and low accessibility (see supplementary Section 6.1 for further discussion of MIF).

3.5.2. Mass-dependent fractionation and in vivo demethylation

Stomach, kidney, and spleen had the lowest mean values of δ^{202}Hg with -0.38 ± 0.33, -0.66 ± 0.30 and -0.97 ± 0.28‰ respectively, which were all negative, while all other tissues had positive mean δ^{202}Hg values. Heart and lean muscle had the highest values of 0.68 ± 0.11 and 0.84 ± 0.2‰, respectively (Table 1, Fig. 2). In addition, a good correlation between δ^{202}Hg and %MeHg was found ($R=0.89$, $p < 0.001$)(Fig. 3) and also patterns in single individuals followed the same trends (Fig. S4). In mammals, lighter isotopes are favored in the demethylation process [31], and internal demethylation activity will result in a net lower δ^{202}Hg in tissues with a high demethylation activity or storage of its products. The final product is suggested to be biomineralized particulate HgSe, as found in marine mammals and birds [36], and in the present study also in different organs of fish.

Earlier studies argued that a lower δ^{202}Hg in liver compared to muscle might be due to lower %MeHg in liver, as IHg was shown to have lower δ^{202}Hg than MeHg in environmental samples and that the change in δ^{202}Hg happened before entering the fish [40]. However, in environmental samples, Δ^{199}Hg was changed simultaneously, which also should change the Δ^{199}Hg in organs, which we did not observe here. Also, we do not expect that the IHg detected at high concentrations in several of the investigated organs originates from dietary intake in a pelagic predator. As discussed earlier, our high %MeHg in liver suggests that investigated ABFT were not foraging in a heavily contaminated environment, and therefore no significant dietary exposure to IHg is expected. And even if so, it has been shown that ingested IHg may not be distributed to other than intestinal organs [82] and is excreted rather rapidly from biological tissue [83].

Investigations on demethylation of MeHg in fish are not consistent and arrive at different conclusions, while evidence for demethylation has been increasing over the last decade. In freshwater fish, Wang et al. [84] did not detect demethylation and instead, methylation of Hg was observed. In a marine fish species, however, an exposure study with dietary MeHg exposure provided strong evidence for demethylation taking place *in vivo* [47]. Using Hg speciation by HR-XANES spectroscopy, Manceau et al. [29] detected $Hg(Sec)_4$ in the liver, but not muscle of freshwater fish and considered *in vivo* demethylation as the most direct interpretation of their findings. Laboratory feeding experiments measuring Hg stable isotope signatures mainly found equilibration to food, indicating absence of internal demethylation in fish [37-40]. The actual observed small scale differences were attributed to the different amounts of MeHg, with higher δ^{202}Hg and Δ^{199}Hg in natural environmental samples compared to IHg [85,86]. Yang et al. [41] reported MIF between liver and muscle of the same individuals of *Notothenia coriiceps* while MDF was constant, and attribute the changes to the specific accumulation of MeHg and IHg rather than internal processes. A positive shift in δ^{202}Hg in liver was found in a feeding experiment by Lee et al. [40]. However, they attributed the positive δ^{202}Hg to the preferential redistribution of IHg with lower δ^{202}Hg rather than demethylation in the fish. Feng et al. [37] observed a consistent Δ^{199}Hg and a much lower δ^{202}Hg in the feces of fish fed with pellets compared to the estimated δ^{202}Hg of IHg in the food and proposed this to be due to MDF possibly *via* internal demethylation. As this was not seen in the tissues, it was argued that potential MDF may be diluted by the isotopic composition of the MeHg in food, which is efficiently assimilated and integrated into various fish tissues [37]. In two field studies on large predatory species, a difference in δ^{202}Hg between muscle and liver was found, while Δ^{199}Hg was constant, indicating internal demethylation [44,45]. Also a controlled MeHg exposure study with European seabass concluded on that demethylation was happening, due to a negative shift and changes in the turnover rate of δ^{202}Hg [43]. Considering isotopic changes in both IHg and MeHg, Wang et al. [46] also found indications of demethylation in fish. In two sympatric shark species, a difference of more than 1 ‰ δ^{202}Hg in muscle of these predators compared to their preys may also indicate *in vivo* MeHg demethylation [42]. Lower Δ^{199}Hg/δ^{202}Hg slopes in muscle of adult pacific bluefin tuna compared to juveniles might also be explained by *in vivo* demethylation if the demethylation would increase significantly with age [87].

Compared to the span of MDF of ~3 ‰ in δ^{202}Hg observed in aquatic mammals across different tissues (brain, muscle, heart, intestine, diaphragm, pancreas, and hair) [25,33,88,31], the span found in ABFT is smaller with 1.81 ‰ in δ^{202}Hg. Also for tusk, where liver and muscle tissues were measured, a difference of on average 1 ‰ in δ^{202}Hg was

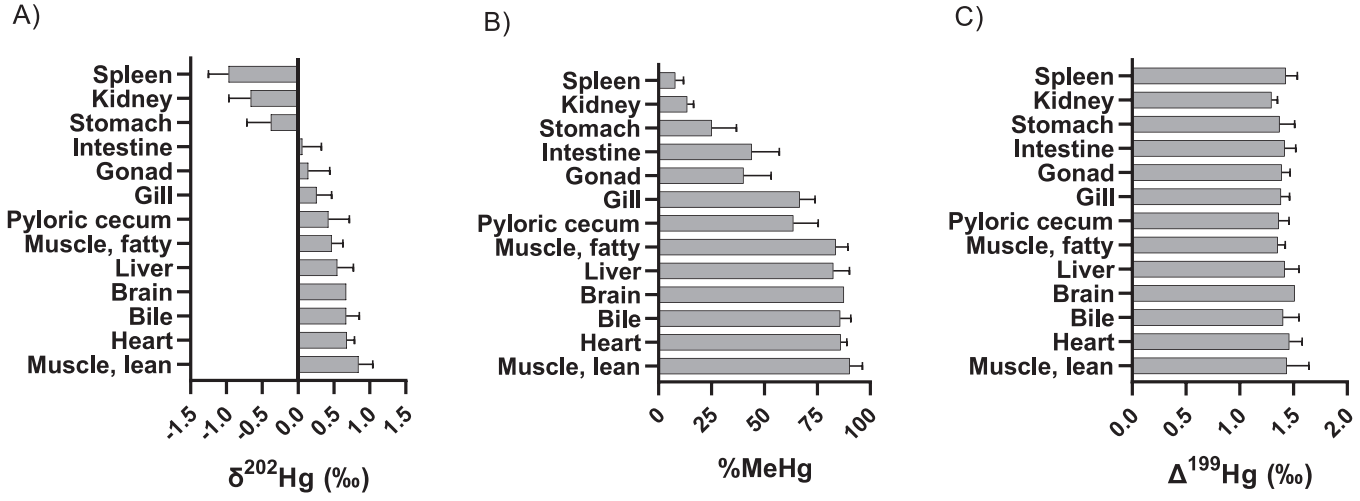

Fig. 2. Mass dependent fractionation (δ^{202}Hg [‰]) and mass independent fractionation (Δ^{199}Hg [‰]) in different organs of Atlantic bluefin tuna caught at the Norwegian coast.

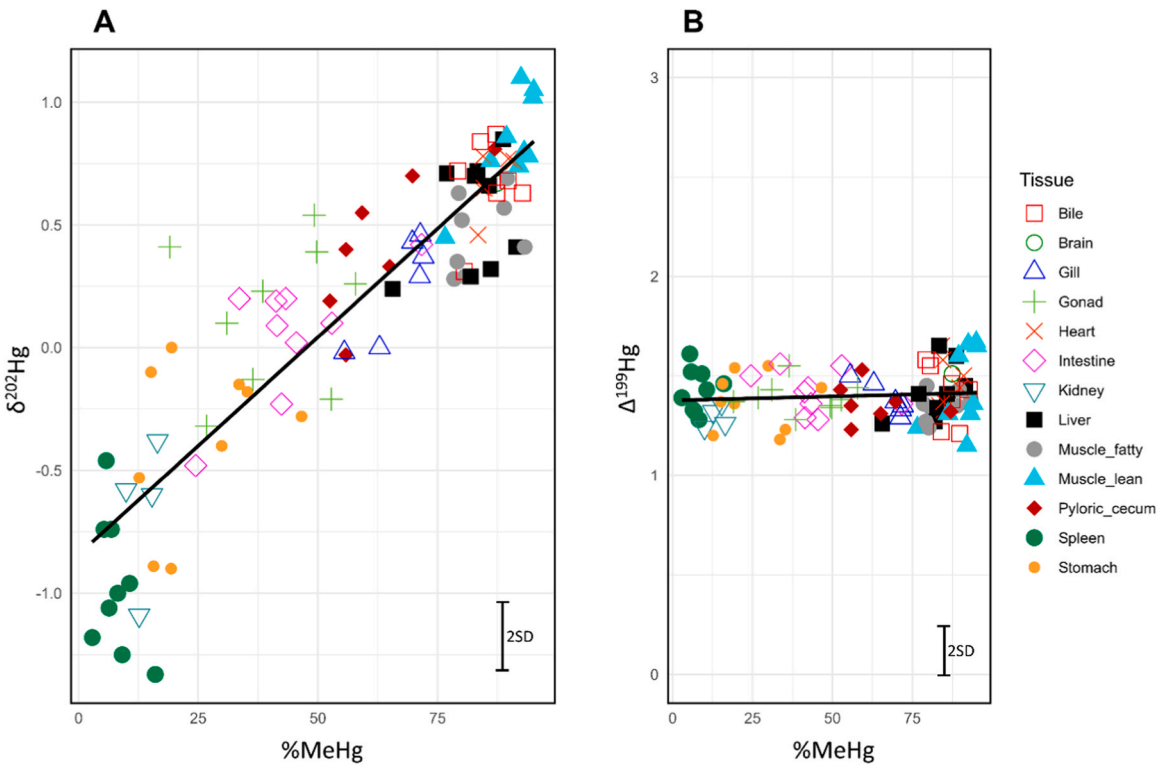

Fig. 3. A: Mass dependent fractionation (δ202Hg [‰]) and B: mass independent fractionation (Δ199Hg [‰]) *versus* the ratio of methylmercury to total mercury (% MeHg) in multiple organs of Atlantic bluefin tuna caught at the Norwegian coast. The error bars show the uncertainty regarding the measured reference material (NIST 8610).

found between the two tissue types [45], similar to European seabass, with an observed maximum of 1.08 ‰ [44]. For ABFT the difference between muscle and liver δ^{202}Hg was insignificant ($p = 0.37$) and averaged 0.3 ‰. The lower net extent of MDF in ABFT compared to mammals might be due to lower THg accumulation levels and therefore less detoxification activity. Manceau et al. [29] reported in freshwater fish, birds and earthworm $Hg(Sec)_4$ as precursor before biomineralization, suggesting a similar mechanism of demethylation in the different phyla. However, for fish, studies quantifying the according changes in δ^{202}Hg are absent making it difficult to disentangle the net change in δ^{202}Hg as a result of the two steps. Applying the regularized inversion calculation, as introduced by Manceau et al. [89], to infer the δ^{202} and fractions of the Hg species in different organs of pilot whale based on measured δ^{202}THg and %MeHg, resulted in inconsistent much lower calculated %HgSe than our actually measured %pHg in kidney and spleen. For giant petrel, an average δ^{202}Hg shift between MeHg and Hg (Sec) of − 4.1 ‰ was reported followed by + 1.6 ‰ during biomineralization [34] applying mathematical inversion of isotopic and spectroscopic data, and validated by δ^{202}MeHg measurements on a subset of tissues. For the same species and samples, applying species-specific isotopic measurement of HgSe particles, Queipo-Abad et al. [68] also observed a negative δ^{202}Hg shift of 2–3 ‰ during demethylation, but found no isotopic fractionation during biomineralization. This highlights the need for further studies on the stepwise shift of δ^{202}Hg caused by Hg detoxification to understand net changes in δ^{202}Hg in different phyla.

In pilot whales, stable isotope data of Hg suggested that HgSe biomineralization and the redistribution of IHg, rather than demethylation is forming the variation in δ^{202}Hg seen in the liver at late life stages [25, 88]. Mercury accumulated with age in whale liver, and it was suggested that the more labile IHg with a lower δ^{202}Hg is exported to other organs, increasing the δ^{202}Hg in the residual THg in old whales. The relatively high δ^{202}Hg found in ABFT liver might result from a similar mechanism of redistribution of Hg as a protective measure against Hg toxicity in liver as observed in zebrafish liver, and accompanied by enrichment in heavier Hg isotopes [37], covering the decrease of δ^{202}Hg due to internal demethylation. Decreasing THg and MeHg concentrations in liver of freshwater tilapia in the depuration phase of an exposure study was also suggested to be due to redistribution of MeHg and THg from liver to other organs, especially muscle [84]. Assuming the stepwise detoxification mechanism of MeHg in fish including demethylation followed by biomineralization accompanied by first a decrease and afterwards increase of δ^{202}Hg during biomineralization [33], another explanation is possible: Even though demethylation takes place in the liver, the biomineralization process may be dominant in liver tissue and therefore increase δ^{202}Hg in the large ABFT investigated here. However, we found high concentrations of particulate Hg in kidney and spleen with the lowest δ^{202}Hg values, suggesting high demethylation activity or deposition of its products in these organs. Suzuki et al. [48], only analyzing muscle tissue suggested that particle formation is occurring regardless of the degree of demethylation in the respective organs, as they did not detect a dependency of the formation of Hg containing particles with THg muscle concentration in different fish species. We found the highest %pHg and %pSe in tissues with the lowest δ^{202}Hg, indicating higher potential demethylation activity.

Our results highlight the organ specificity of Hg detoxification and that simultaneously investigating several organs is a useful approach. Wang et al. [47] found that contrary to earlier suspicions of liver being the main site for demethylation, as a main detoxification organ, the intestine may play a more important role. In a recent study on cuttlefish, the highest rate of *in vivo* MeHg demethylation was found in digestive gland, and low activity in gut [90]. In whales, kidney and liver δ^{202}Hg were rather similar [25], while we found a large difference in ABFT. Future investigations regarding metabolic processes and cycling of Hg in biota will benefit from considering a more diverse array of organs compared to simply focusing on muscle tissue and liver. Furthermore, the differences in δ^{202}Hg between liver and muscle, together with the varying content of %MeHg in the liver in different fish species suggests

that the metabolic processes involved in Hg cycling are also highly context and species specific. Collectively, these data suggest that different species rely on different organs to support MeHg detoxification, and that demethylation of MeHg is a widespread phenomenon in nature [29].

4. Conclusions

The application of organ-specific Hg and Se speciation determination, Hg stable isotope analysis and Hg and Se particle measurements in several different tissues provided further understanding of Hg metabolism dynamics in ABFT. While mass dependent fractionation (denoted by δ^{202}Hg) was bidirectionally affected by *in vivo* demethylation in the different tissues, mass independent fractionation (denoted by Δ^{199}Hg) was stable. Furthermore, we detected particulate Hg and Se in the organs with a high demethylation activity, and in lower numbers in muscle, where no demethylation was expected, as indicated by the Hg stable isotope signature. Collectively, our data provide evidence of organ specific *in vivo* MeHg demethylation in ABFT with an involvement of spleen and kidney. This suggests similar metabolic processing of Hg as reported for marine mammals and waterbirds with a two-step detoxification process including demethylation of MeHg followed by biomineralization of particulate HgSe. MeHg detoxification was highly organ specific, and hence, considering multiple tissues is important for mechanistic understanding. Further research is needed on the role of liver and sequence of demethylation and biomineralization and storage of the products in the different organs. Additionally, the low observed variability of organ specific Δ^{199}Hg values suggested that most tissue types could be used for MIF signature analyses to study source apportionment dynamics.

Environmental implications

In our study we focused on the detoxification of MeHg, considered a legacy contaminant threatening environmental and public health driving fish consumption advisories worldwide. Research on the detoxification mechanisms of MeHg mostly focused on seabirds and marine mammals, and not fish, despite their relevance for public health via seafood consumption and large biomass, and importance for mercury cycling and environmental health. Knowledge on the distribution of Hg and Se particles and mercury speciation in biota is important for the implementation of Hg monitoring, and data on Hg isotope signatures is needed for the interpretation of source apportionment to pursuit the risk posed by MeHg.

CRediT authorship contribution statement

Martin Wiech: Writing – original draft, Visualization, Resources, Project administration, Investigation, Funding acquisition, Conceptualization. **André M. Bienfait:** Writing – review & editing, Visualization, Investigation, Formal analysis, Conceptualization. **Marta Silva:** Writing – review & editing, Visualization, Investigation, Formal analysis. **Julien Barre:** Writing – review & editing, Formal analysis. **Veronika Sele:** Writing – review & editing, Visualization, Investigation, Formal analysis. **Michael S. Bank:** Writing – review & editing, Investigation, Formal analysis, Conceptualization. **Sylvain Bérail:** Writing – review & editing, Formal analysis. **Emmanuel Tessier:** Writing – review & editing, Investigation, Formal analysis. **David Amouroux:** Writing – review & editing, Formal analysis. **Atabak M. Azad:** Writing – review & editing, Visualization, Investigation, Formal analysis, Conceptualization.

Declaration of Competing Interest

The authors declare that they have no known competing financial interests or personal relationships that could have appeared to influence the work reported in this paper.

Data Availability

Data will be made available on request.

Acknowledgements

We would like to express our gratitude to the recreational fishers, Sigurd Øyan and the tuna tagging team at the Institute of Marine Research, Bergen for their help providing and collecting samples of the ABFT. Thanks to Kjersti Vaksdal for her help with the selenium speciation analysis. The investigation was funded by the Norwegian Ministry of Trade, Industry and Fisheries and supported from the European Union's Horizon 2020 research and innovation MSCA-RISE program under grant agreement No. 101007962 (merfish.eu).

Appendix A. Supporting information

Supplementary data associated with this article can be found in the online version at doi:10.1016/j.jhazmat.2024.134699.

References

[1] Cáceres-Saez, I., Haro, D., Blank, O., Lobo, A.A., Dougnac, C., Arredondo, C., et al., 2018. High status of mercury and selenium in false killer whales (*Pseudorca crassidens*, Owen 1846) stranded on Southern South America: a possible toxicological concern? Chemosphere 199, 637–646.
[2] Clarkson, T.W., Magos, L., 2006. The toxicology of mercury and its chemical compounds. Crit Rev Toxicol 36 (8), 609–662.
[3] Scheuhammer, A., Braune, B., Chan, H.M., Frouin, H., Krey, A., Letcher, R., et al., 2015. Recent progress on our understanding of the biological effects of mercury in fish and wildlife in the Canadian Arctic. Sci Total Environ 509, 91–103.
[4] Bank, M.S., Chesney, E., Shine, J.P., Maage, A., Senn, D.B., 2007. Mercury bioaccumulation and trophic transfer in sympatric snapper species from the Gulf of Mexico. Ecol Appl 17 (7), 2100–2110.
[5] Bank, M.S., Frantzen, S., Duinker, A., Amouroux, D., Tessier, E., Nedreaas, K., et al., 2021. Rapid temporal decline of mercury in Greenland halibut (*Reinhardtius hippoglossoides*). Environ Pollut 289, 117843.
[6] Bank, M.S., Ho, Q.T., Ingvaldsen, R.B., Duinker, A., Nilsen, B.M., Maage, A., et al., 2023. Climate change dynamics and mercury temporal trends in Northeast Arctic cod (*Gadus morhua*) from the Barents Sea ecosystem. Environ Pollut 338, 122706.
[7] Bloom, N.S., 1992. On the chemical form of mercury in edible fish and marine invertebrate tissue. Can J Fish Aquat Sci 49 (5), 1010–1017.
[8] Bravo, A.G., Cosio, C., 2020. Biotic formation of methylmercury: a bio–physico–chemical conundrum. Limnol Oceanogr 65 (5), 1010–1027.
[9] Celo, V., Lean, D.R., Scott, S.L., 2006. Abiotic methylation of mercury in the aquatic environment. Sci Total Environ 368 (1), 126–137.
[10] Mason, R., Fitzgerald, W., 1991. Mercury speciation in open ocean waters. Waters Water Air Soil Pollut 56, 779–789.
[11] Amlund, H., Lundebye, A.-K., Berntssen, M.H., 2007. Accumulation and elimination of methylmercury in Atlantic cod (*Gadus morhua* L.) following dietary exposure. Aquat Toxicol 83 (4), 323–330.
[12] Bosch, A.C., O'Neill, B., Sigge, G.O., Kerwath, S.E., Hoffman, L.C., 2016. Mercury accumulation in Yellowfin tuna (*Thunnus albacares*) with regards to muscle type, muscle position and fish size. Food Chem 190, 351–356.
[13] Lavoie, R.A., Hebert, C.E., Rail, J.F., Braune, B.M., Yumvihoze, E., Hill, L.G., et al., 2010. Trophic structure and mercury distribution in a Gulf of St. Lawrence (Canada) food web using stable isotope analysis. Sci Total Environ 408 (22), 5529–5539. https://doi.org/10.1016/j.scitotenv.2010.07.053.
[14] Lavoie, R.A., Jardine, T.D., Chumchal, M.M., Kidd, K.A., Campbell, L.M., 2013. Biomagnification of mercury in aquatic food webs: a worldwide meta-analysis. Environ Sci Technol 47 (23), 13385–13394.
[15] Block, B.A., Dewar, H., Blackwell, S.B., Williams, T.D., Prince, E.D., Farwell, C.J., et al., 2001. Migratory movements, depth preferences, and thermal biology of Atlantic bluefin tuna. Science 293 (5533), 1310–1314.
[16] Santamaria, N., Bello, G., Corriero, A., Deflorio, M., Vassallo-Agius, R., Bök, T., et al., 2009. Age and growth of Atlantic bluefin tuna, *Thunnus thynnus* (Osteichthyes: Thunnidae), in the Mediterranean Sea. J Appl Ichthyol 25 (1), 38–45.
[17] Annibaldi, A., Truzzi, C., Carnevali, O., Pignalosa, P., Api, M., Scarponi, G., et al., 2019. Determination of Hg in farmed and wild atlantic bluefin tuna (*Thunnus thynnus* L.) muscle. Molecules 24 (7), 1273.
[18] Lee, C.-S., Lutcavage, M.E., Chandler, E., Madigan, D.J., Cerrato, R.M., Fisher, N.S., 2016. Declining mercury concentrations in bluefin tuna reflect reduced emissions to the North Atlantic Ocean. Environ Sci Technol 50 (23), 12825–12830.
[19] Tseng, C.-M., Ang, S.-J., Chen, Y.-S., Shiao, J.-C., Lamborg, C.H., He, X., et al., 2021. Bluefin tuna reveal global patterns of mercury pollution and bioavailability in the world's oceans. Proc Natl Acad Sci 118 (38), e2111205118.
[20] EFSA, P. o C. i t F.C., 2012. Scientific opinion on the risk for public health related to the presence of mercury and methylmercury in food. EFSA J 10 (12), 2985.

[21] Rice, G., Swartout, J., Mahaffey, K., Schoeny, R., 2000. Derivation of US EPA's oral Reference Dose (RfD) for methylmercury. Drug Chem Toxicol 23 (1), 41–54.
[22] Pereira, P., Korbas, M., Pereira, V., Cappello, T., Maisano, M., Canario, J., et al., 2019. A multidimensional concept for mercury neuronal and sensory toxicity in fish-From toxicokinetics and biochemistry to morphometry and behavior. Biochim Et Biophys Acta (BBA)-Gen Subj 1863 (12), 129298.
[23] Harris, H.H., Pickering, I.J., George, G.N., 2003. The chemical form of mercury in fish. Science 301 (5637), 1203-1203.
[24] Lemes, M., Wang, F., 2009. Methylmercury speciation in fish muscle by HPLC-ICP-MS following enzymatic hydrolysis. J Anal Spectrom 24 (5), 663–668.
[25] Bolea-Fernandez, E., Rua-Ibarz, A., Krupp, E.M., Feldmann, J., Vanhaecke, F., 2019. High-precision isotopic analysis sheds new light on mercury metabolism in long-finned pilot whales (*Globicephala melas*). Sci Rep 9 (1), 1–10.
[26] Gajdosechova, Z., Lawan, M.M., Urgast, D.S., Raab, A., Scheckel, K.G., Lombi, E., et al., 2016. In vivo formation of natural HgSe nanoparticles in the liver and brain of pilot whales. Sci Rep 6 (1), 1–11.
[27] Palmisano, F., Cardellicchio, N., Zambonin, P., 1995. Speciation of mercury in dolphin liver: a two-stage mechanism for the demethylation accumulation process and role of selenium. Mar Environ Res 40 (2), 109–121.
[28] Eagles-Smith, C.A., Ackerman, J.T., Yee, J., Adelsbach, T.L., 2009. Mercury demethylation in waterbird livers: dose–response thresholds and differences among species. Environ Toxicol Chem Int J 28 (3), 568–577.
[29] Manceau, A., Bourdineaud, J.-P., Oliveira, R.B., Sarrazin, S.L., Krabbenhoft, D.P., Eagles-Smith, C.A., et al., 2021. Demethylation of methylmercury in bird, fish, and earthworm. Environ Sci Technol 55 (3), 1527–1534.
[30] Renedo, M., Pedrero, Z., Amouroux, D., Cherel, Y., Bustamante, P., 2021. Mercury isotopes of key tissues document mercury metabolic processes in seabirds. Chemosphere 263, 127777.
[31] Perrot, V., Masbou, J., Pastukhov, M.V., Epov, V.N., Point, D., Bérail, S., et al., 2016. Natural Hg isotopic composition of different Hg compounds in mammal tissues as a proxy for *in vivo* breakdown of toxic methylmercury. Metallomics 8 (2), 170–178.
[32] Sherman, L.S., Blum, J.D., Franzblau, A., Basu, N., 2013. New insight into biomarkers of human mercury exposure using naturally occurring mercury stable isotopes. Environ Sci Technol 47 (7), 3403–3409.
[33] Li, M.-L., Kwon, S.Y., Poulin, B.A., Tsui, M.T.-K., Motta, L.C., Cho, M., 2022. Internal dynamics and metabolism of mercury in biota: A review of insights from mercury stable isotopes. Environ Sci Technol 56 (13), 9182–9195.
[34] Manceau, A., Brossier, R., Janssen, S.E., Rosera, T.J., Krabbenhoft, D.P., Cherel, Y., et al., 2021. Mercury isotope fractionation by internal demethylation and biomineralization reactions in seabirds: Implications for environmental mercury science. Environ Sci Technol 55 (20), 13942–13952.
[35] Manceau, A., Azemard, S., Hédouin, L., Vassileva, E., Lecchini, D., Fauvelot, C., et al., 2021. Chemical forms of mercury in blue marlin billfish: implications for human exposure. Environ Sci Technol Lett 8 (5), 405–411.
[36] Ji, X., Yang, L., Wu, F., Yao, L., Yu, B., Liu, X., et al., 2022. Identification of mercury-containing nanoparticles in the liver and muscle of cetaceans. J Hazard Mater 424, 127759.
[37] Feng, C., Pedrero, Z., Gentès, S., Barre, J., Renedo, M., Tessier, E., et al., 2015. Specific pathways of dietary methylmercury and inorganic mercury determined by mercury speciation and isotopic composition in zebrafish (*Danio rerio*). Environ Sci Technol 49 (21), 12984–12993.
[38] Kwon, S.Y., Blum, J.D., Chirby, M.A., Chesney, E.J., 2013. Application of mercury isotopes for tracing trophic transfer and internal distribution of mercury in marine fish feeding experiments. Environ Toxicol Chem 32 (10), 2322–2330.
[39] Kwon, S.Y., Blum, J.D., Madigan, D.J., Block, B.A., Popp, B.N., 2016. Quantifying mercury isotope dynamics in captive Pacific bluefin tuna (*Thunnus orientalis*) Mercury isotope dynamics in Pacific bluefin tuna. Elem: Sci Anthr 4, 000088.
[40] Lee, B.J., Kwon, S.Y., Yin, R., Li, M., Jung, S., Lim, S.H., et al., 2020. Internal dynamics of inorganic and methylmercury in a marine fish: Insights from mercury stable isotopes. Environ Pollut 267, 115588.
[41] Yang, L., Yu, B., Liu, H., Ji, X., Xiao, C., Cao, M., et al., 2023. Foraging behavior and sea ice-dependent factors affecting the bioaccumulation of mercury in Antarctic coastal waters. Sci Total Environ, 169557.
[42] Le Croizier, G., Lorrain, A., Sonke, J.E., Jaquemet, S., Schaal, G., Renedo, M., et al., 2020. Mercury isotopes as tracers of ecology and metabolism in two sympatric shark species. Environ Pollut 265, 114931.
[43] Pinzone, M., Cransveld, A., De Boeck, G., Shrivastava, J., Tessier, E., Bérail, S., et al., 2022. Dynamics of dietary mercury determined by mercury speciation and isotopic composition in *Dicentrarchus labrax*. Front Environ Chem 3, 767202.
[44] Pinzone, M., Cransveld, A., Tessier, E., Bérail, S., Schnitzler, J., Das, K., et al., 2021. Contamination levels and habitat use influence Hg accumulation and stable isotope ratios in the European seabass *Dicentrarchus labrax*. Environ Pollut 281, 117008.
[45] Rua-Ibarz, A., Bolea-Fernandez, E., Maage, A., Frantzen, S., Sanden, M., Vanhaecke, F., 2019. Tracing Mercury Pollution along the Norwegian Coast via Elemental, Speciation, and Isotopic Analysis of Liver and Muscle Tissue of Deep-Water Marine Fish (*Brosme brosme*). Environ Sci Technol 53 (4), 1776–1785.
[46] Wang, B., Yang, S., Li, P., Qin, C., Wang, C., Ali, M.U., et al., 2023. Trace mercury migration and human exposure in typical mercury-emission areas by compound-specific stable isotope analysis. Environ Int 174, 107891.
[47] Wang, X., Wu, F., Wang, W.-X., 2017. *In vivo* Mercury Demethylation in a Marine Fish. Environ Sci Technol 51 (11), 6441–6451.
[48] Suzuki, Y., Kondo, M., Akiyama, H., Ogra, Y., 2022. Presence of nano-sized mercury-containing particles in seafoods, and an estimate of dietary exposure. Environ Pollut 307, 119555.
[49] Cort, J.L., Estruch, V.D., 2019. Review of recent studies on the absolute and relative growth of Atlantic bluefin tuna: Similarities with the Pacific bluefin tuna. Rev Fish Sci Aquac 27 (1), 88–105.
[50] Vacchina, V., Dumont, J., 2018. Total selenium quantification in biological samples by inductively coupled plasma mass spectrometry (ICP-MS). Selenoproteins: Methods and Protocols. Humana Press, New York, NY.
[51] Clémens, S., Monperrus, M., Donard, O.F., Amouroux, D., Guérin, T., 2011. Mercury speciation analysis in seafood by species-specific isotope dilution: method validation and occurrence data. Anal Bioanal Chem 401, 2699–2711.
[52] Rodriguez Martin-Doimeadios, R., Krupp, E., Amouroux, D., Donard, O.F.X., 2002. Application of isotopically labeled methylmercury for isotope dilution analysis of biological samples using gas chromatography/ICPMS. Anal Chem 74 (11), 2505–2512.
[53] Rodríguez-González, P., Monperrus, M., Alonso, J.G., Amouroux, D., Donard, O.F., 2007. Comparison of different numerical approaches for multiple spiking species-specific isotope dilution analysis exemplified by the determination of butyltin species in sediments. J Anal Spectrom 22 (11), 1373–1382.
[54] Bruvold, A., Valdersnes, S., Loeschner, K., Bienfait, A.M., 2024. Validation of a method for surveillance of nanoparticles in mussels using single particle inductively coupled plasma mass spectrometry. J AOAC Int, qsae024.
[55] Sele, V., Ørnsrud, R., Sloth, J.J., Berntssen, M.H., Amlund, H., 2018. Selenium and selenium species in feeds and muscle tissue of Atlantic salmon. J Trace Elem Med Biol 47, 124–133.
[56] Vaksdal, K.E.L. (2021). Optimization of Analytical Method for Selenium Speciation in Fish Feed and Feed Ingredients Using a Chemometric Approach. (Master). University of Bergen, Retrieved from ⟨https://bora.uib.no/bora-xmlui/handle/11250/2737655⟩.
[57] Julshamn, K., Maage, A., Norli, H.S., Grobecker, K.H., Jorhem, L., Fecher, P., et al., 2007. Determination of arsenic, cadmium, mercury, and lead by inductively coupled plasma/mass spectrometry in foods after pressure digestion: NMKL interlaboratory study. J AOAC Int 90 (3), 844–856.
[58] Blum, J.D., Bergquist, B.A., 2007. Reporting of variations in the natural isotopic composition of mercury. Anal Bioanal Chem 388, 353–359.
[59] Bergquist, B.A., Blum, J.D., 2007. Mass-dependent and-independent fractionation of Hg isotopes by photoreduction in aquatic systems. Science 318 (5849)), 417–420.
[60] Masbou, J., Point, D., Sonke, J.E., 2013. Application of a selective extraction method for methylmercury compound specific stable isotope analysis (MeHg-CSIA) in biological materials. J Anal Spectrom 28 (10), 1620–1628.
[61] Sherman, L.S., Blum, J.D., 2013. Mercury stable isotopes in sediments and largemouth bass from Florida lakes, USA. Sci Total Environ 448, 163–175.
[62] European Commission, 2023. Commission Regulation (EU) 2023/915 of 25 April 2023 on maximum levels for certain contaminants in food and repealing Regulation (EC) No 1881/2006. In: Off. J. Eur. Union, 119, pp. 103–157.
[63] Rodríguez-Ezpeleta, N., Díaz-Arce, N., Walter III, J.F., Richardson, D.E., Rooker, J. R., Nøttestad, L., et al., 2019. Determining natal origin for improved management of Atlantic bluefin tuna. Front Ecol Environ 17 (8), 439–444.
[64] Drevnick, P.E., Roberts, A.P., Otter, R.R., Hammerschmidt, C.R., Klaper, R., Oris, J. T., 2008. Mercury toxicity in livers of northern pike (*Esox lucius*) from Isle Royale, USA. Comp Biochem Physiol Part C: Toxicol Pharmacol 147 (3), 331–338.
[65] Chumchal, M.M., Rainwater, T.R., Osborn, S.C., Roberts, A.P., Abel, M.T., Cobb, G. P., et al., 2011. Mercury speciation and biomagnification in the food web of Caddo Lake, Texas and Louisiana, USA, a subtropical freshwater ecosystem. Environ Toxicol Chem 30 (5), 1153–1162.
[66] Oliveira Ribeiro, C.A., Rouleau, C., Pelletier, E., Audet, C., Tjälve, H., 1999. Distribution kinetics of dietary methylmercury in the arctic charr (*Salvelinus alpinus*). Environ Sci Technol 33 (6), 902–907.
[67] Azad, A.M., Frantzen, S., Bank, M.S., Nilsen, B.M., Duinker, A., Madsen, L., et al., 2019. Effects of geography and species variation on selenium and mercury molar ratios in Northeast Atlantic marine fish communities. Sci Total Environ 652, 1482–1496.
[68] Queipo-Abad, S., Pedrero, Z., Marchán-Moreno, C., El Hanafi, K., Bérail, S., Corns, W.T., et al., 2022. New insights into the biomineralization of mercury selenide nanoparticles through stable isotope analysis in giant petrel tissues. J Hazard Mater 425, 127922.
[69] Nakazawa, E., Ikemoto, T., Hokura, A., Terada, Y., Kunito, T., Tanabe, S., et al., 2011. The presence of mercury selenide in various tissues of the striped dolphin: evidence from μ-XRF-XRD and XAFS analyses. Metallomics 3 (7), 719–725.
[70] von Hellfeld, R., Gade, C., Ten Doeschate, M., Davison, N.J., Brownlow, A., Mbadugha, L., et al., 2023. High resolution visualisation of tiemannite microparticles, essential in the detoxification process of mercury in marine mammals. Environ Pollut, 123027.
[71] Takahashi, K., Encinar, J.R., Costa-Fernández, J.M., Ogra, Y., 2021. Distributions of mercury and selenium in rats ingesting mercury selenide nanoparticles. Ecotoxicol Environ Saf 226, 112867.
[72] Kumar, K., Saxena, P.N., 2020. Mercury selenide nanoparticles induced toxicity on LDL, VLDL and Cholesterol-HDL ratio of *Rattus norvegicus*. Mater Today Proc 31, 646–650.
[73] Saxena, P.N., Rawat, G., & Awasthi, K. (2015). *Mercury Selenide Nanoparticles Induced Immunological Alterations in Male Wistar Rat*. Paper presented at the Proceedings of the the World Congress on New Technologies.
[74] Singhato, A., Judprasong, K., Sridonpai, P., Laitip, N., Ornthai, N., Yafa, C., 2023. Speciation of selenium in fresh and cooked commonly consumed fish in Thailand. J Food Compos Anal 120, 105303.
[75] Ralston, N.V., Azenkeng, A., Raymond, L.J., 2012. Mercury-dependent inhibition of selenoenzymes and mercury toxicity. Methylmercury Neurotox 91–99.

[76] Lall, S.P., Kaushik, S.J., 2021. Nutrition and metabolism of minerals in fish. Animals 11 (09), 2711.
[77] Bryszewska, M.A., Måge, A., 2015. Determination of selenium and its compounds in marine organisms. J Trace Elem Med Biol 29, 91–98.
[78] Yamashita, Y., Amlund, H., Suzuki, T., Hara, T., Hossain, M.A., Yabu, T., et al., 2011. Selenoneine, total selenium, and total mercury content in the muscle of fishes. Fish Sci 77, 679–686.
[79] Bierla, K., Szpunar, J., Lobinski, R., Sunde, R.A., 2023. Selenomethionine supplementation and expression of selenosugars, selenocysteine, and other selenometabolites in rat liver. Metallomics 15 (11) mfad067.
[80] Blum, J.D., Sherman, L.S., Johnson, M.W., 2014. Mercury isotopes in earth and environmental sciences. Annu Rev Earth Planet Sci 42, 249–269.
[81] Poulin, B.A., Janssen, S.E., Rosera, T.J., Krabbenhoft, D.P., Eagles-Smith, C.A., Ackerman, J.T., et al., 2021. Isotope fractionation from *in vivo* methylmercury detoxification in waterbirds. ACS Earth Space Chem 5 (5), 990–997.
[82] Oliveira Ribeiro, C.A., Belger, L., Pelletier, E., Rouleau, C., 2002. Histopathological evidence of inorganic mercury and methyl mercury toxicity in the arctic charr (*Salvelinus alpinus*). Environ Res 90 (3), 217–225.
[83] Cizdziel, J., Hinners, T., Cross, C., Pollard, J., 2003. Distribution of mercury in the tissues of five species of freshwater fish from Lake Mead. Usa J Environ Monit 5 (5), 802–807.
[84] Wang, R., Feng, X.-B., Wang, W.-X., 2013. *In vivo* mercury methylation and demethylation in freshwater tilapia quantified by mercury stable isotopes. Environ Sci Technol 47 (14), 7949–7957.
[85] Entwisle, J., Malinovsky, D., Dunn, P.J., Goenaga-Infante, H., 2018. Hg isotope ratio measurements of methylmercury in fish tissues using HPLC with off line cold vapour generation MC-ICPMS. J Anal Spectrom 33 (10), 1645–1654.
[86] Janssen, S.E., Johnson, M.W., Blum, J.D., Barkay, T., Reinfelder, J.R., 2015. Separation of monomethylmercury from estuarine sediments for mercury isotope analysis. Chem Geol 411, 19–25.
[87] He, X., Chen, Y.S., Ang, S.J., Shiao, J.C., Tseng, C.M., Reinfelder, J.R., 2023. Mercury stable isotopes reveal sources of methylmercury and prey in giant Pacific bluefin tuna from the western North Pacific Ocean. Limnol Oceanogr Lett 481–489.
[88] Li, M., Juang, C.A., Ewald, J.D., Yin, R., Mikkelsen, B., Krabbenhoft, D.P., et al., 2020. Selenium and stable mercury isotopes provide new insights into mercury toxicokinetics in pilot whales. Sci Total Environ 710, 136325.
[89] Manceau, A., Brossier, R., Poulin, B.A., 2021. Chemical forms of mercury in pilot whales determined from species-averaged mercury isotope signatures. ACS Earth Space Chem 5 (6), 1591–1599.
[90] Gentès, S., Minet, A., Lopes, C., Tessier, E., Gassie, C., Guyoneaud, R., et al., 2023. *In Vivo* mercury (De) methylation metabolism in Cephalopods under different pCO_2 scenarios. Environ Sci Technol 57 (14), 5761–5770.